Hybrid Optothermal-Magnetic Mobile Microgripper for in-liquid Micromanipulation

Belal Ahmad, Antoine Barbot, Gwenn Ulliac, Aude Bolopion

Hybrid Optothermal-Magnetic Mobile Microgripper for in-liquid Micromanipulation

Belal Ahmad, *Member, IEEE*, Antoine Barbot, Gwenn Ulliac, and Aude Bolopion, *Member, IEEE*

***Abstract*—In this paper, we propose a mobile microgripper actuated using laser optothermal and magnetic actuation in liquid environments. This hybrid actuation scheme allows the full decoupling between the in-plane positioning of the mobile microgripper and the actuation of its gripping mechanism, which reduces the control complexity of such microgrippers. The developed mobile microgripper with the dimensions of 1500×700×250 µm^3 can realize an open and close gripping motion of 35 µm, a magnetic positioning accuracy of 6 µm for translation over an area of 1×1 mm and 2° for rotation, and a laser steering accuracy of 25 µm. Finally, the mobile microgripper is used to control the position of a microbead inside a liquid environment. Our work provides a proof of concept of laser optothermal-magnetic hybrid actuation, which has the potential to enhance the deployment of microtools in biomedical applications including cell manipulation and lab-on-chip devices.**

***Index Terms*—Micro/nano robots, automation at micro-nano scales, mobile manipulation, magnetic actuation, optothermal actuation**

I. INTRODUCTION

Microgrippers are used to manipulate objects such as microparts in microassembly and biological cells in biomedical applications to name a few [1], [2]. Specifically, mechanical microgrippers offer a number of advantages compared to their noncontact counterparts, such as optical and magnetic tweezers. These advantages include applying higher forces reaching to µN and mN and the ability to design specific end-effectors to either puncture, indent, or gently catch biological entities. Conventional tethered mechanical microgrippers, such as piezoelectric microgrippers, are powered and actuated directly through wires [3]. This tethered scheme limits the maneuverability and reach of such microgrippers, and makes them impractical in applications that require closed environments such as lab-on-chips. On the other hand, mobile microgrippers can be deployed in both open and closed environments with enhanced maneuverability and reach [4]–[6]. These microgrippers need to be actuated remotely with no physical connections to the microgripper. Therefore, a number of actuation techniques have been developed in the literature to remotely transfer a driving energy to the microgripper including magnetic, acoustic, thermal, and optical actuation. One of the difficult challenges that arises when designing a mobile microgripper is the decoupling between the actuation of the body of the microgripper, i.e. positioning, and the actuation of the gripping mechanism. In case of using only one actuation technique, complex control methods to decouple positioning and gripping should be implemented [7], [8].

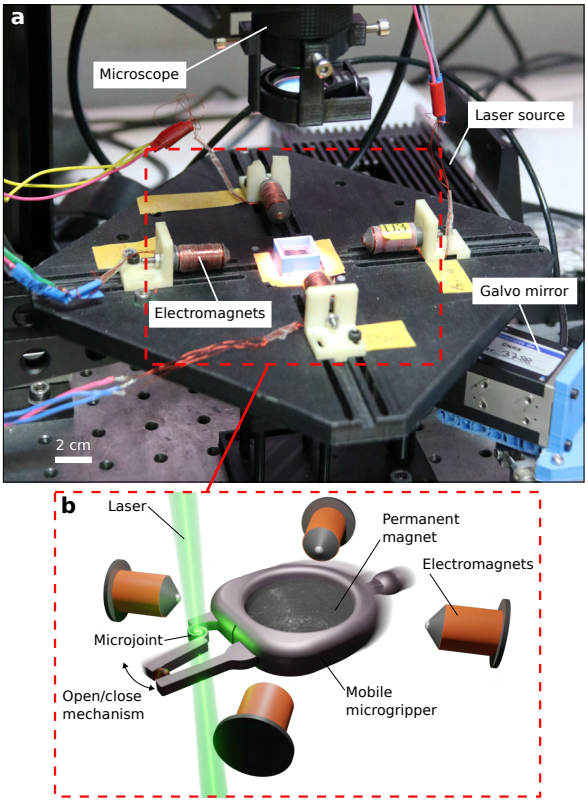

Fig. 1. (a) A picture depicting the physical system. (b) A conceptual image of the proposed hybrid optothermal-magnetic mobile microgripper. The position of the microgripper is magnetically actuated and the gripping mechanism is optothermally actuated. The microgripper is approximately 1.5 mm in length. The conceptual image is not to scale.

Manuscript received: October, 29, 2022; Revised January, 4, 2023; Accepted January, 21, 2023. This paper was recommended for publication by Editor P. Valdastri upon evaluation of the Associate Editor and Reviewers' comments. This work was supported in part by the EIPHI Graduate School under Contract ANR- 17-EURE-0002, in part by the MiMedi project funded by BPI France under Grant DOS0060162/00, and by the European Union through the European Regional Development Fund of the Region Bourgogne-Franche-Comté under Grant FC0013440, in part by the French ROBOTEX network and its FEMTO-ST technological facility under Grant ANR-10-EQPX-44-01, and in part by the french RENATECH network and its FEMTO-ST technological facility.

B. Ahmad, A. Barbot, G. Ulliac, and A. Bolopion are with FEMTO-ST Institute, Univ. Bourgogne Franche-Comté, CNRS, Besançon, France (e-mail: antoine.barbot@femto-st.fr, gwenn.ulliac@femto-st.fr, aude.bolopion@femto-st.fr). Corresponding author: B. Ahmad (email: belal.ahmad@femto-st.fr).

Digital Object Identifier (DOI): see top of this page.

The use of hybrid actuation, i.e. two distinct actuation techniques (Fig. 1), for positioning and gripping is emerging thanks to the rapid development in stimuli-responsive materials. This provides a promising alternative that can reduce the control complexity [9], [10]. Magnetic actuation is the most widely used technique to actuate mobile microrobots and microgrippers owing to its versatility and ease of implementation. Hybrid actuation has mainly been proposed using temperature responsive materials [11]–[14] to control the gripper mechanism. The non-localized nature of thermal actuation causes the whole working environment to be heated, which limits the feasibility of such microgrippers especially in biomedical applications as well as the mechanism response time to heat up and cool down (typically few seconds). Therefore, a remote, localized, and fast actuation technique could allow fast actuation with minimum impact on the environment. Such precise and fast heating can be achieve with optothermal effect where a laser beam is focused at a specific location in an object. This approach has been validated in dry a environment for a hybrid microgripper with magnetic levitation [15] but remain challenging in liquid where thermal dissipation is higher. In this article, we propose a hybrid mobile microgripper in liquid environment which combines magnetic positioning and opthothermal gripper actuation in a fully decoupled scheme. The gripper actuation is based on our previous work on compact opthothermal microjoints demonstrating fast performance in liquid environments [16]. Compared to fully magnetically actuated mobile microgrippers, the proposed approach offers the advantages of reduced control complexity and the potential to allow gripping mechanisms with multiple degrees-of-freedom (DOF), which can enable more functionality of the microgripper in future work. To the best of our knowledge, this work is the first proof of concept utilizing laser optothermal actuation with magnetic actuation to realize a mobile microgripper for micromanipulation applications in liquid environments. The work has a high potential for biomedical applications, such as the manipulation and transfer of a single cell from a pool of cells for further investigation in lab-on-chip devices.

This paper will be organized as follows: In section II, the design, fabrication, and the hybrid optothermal-magnetic control will be shown, including the two dimensional positioning of the microgripper in the working area using magnetic fields and the two dimensional steering of the laser beam using a tip/tilt galvo mirror. In section III, experiments showing the performance of the magnetic and optothermal actuation of the microgripper along with micromanipulation experiment of microbeads will be demonstrated. Finally in section IV, the future directions will be discussed.

II. DESIGN

A. Microgripper Design and Fabrication

The mobile microgripper design and dimensions are shown in Fig. 2(a). The microgripper has the dimensions of 1500×700×250 μm^3. It mainly consists of a body part and a gripper part. The body part contains a circular hole to press fit a permanent magnet to enable its magnetic actuation. In addition, a circular-shaped tail is attached to the body to detect the orientation of the microgripper by image processing. For the gripper part, an optothermally actuated two-fingers design is implemented using a stationary finger and a movable finger. The motion of the movable finger is achieved using our previously proposed optothermal bimaterial microjoint [16]. The microjoint exhibits a rotational motion upon laser heating due to the different thermal expansion coefficients of its two materials, which allows the gripper part to be activated on demand. The design of the gripper part can be modified to suit the size of the target object by tuning the initial gap between its two fingers in the design process. Fig. 2(a) also shows that the height of the press fitted permanent magnet is larger than the height of the microgripper, where the magnet will be in contact with the substrate of the working area to reduce the adhesion thanks to its rough surface. Therefore, the fingers are tilted downwards with a 45° angle to enable the micromanipulation of objects smaller than the total height of the microgripper. In addition, a sawtooth pattern is added to the tip of the fingers to enhance object release by reducing the contact area with the object.

The fabrication and release process of the microgripper is shown in Fig. 2(b). The microgripper was fabri-

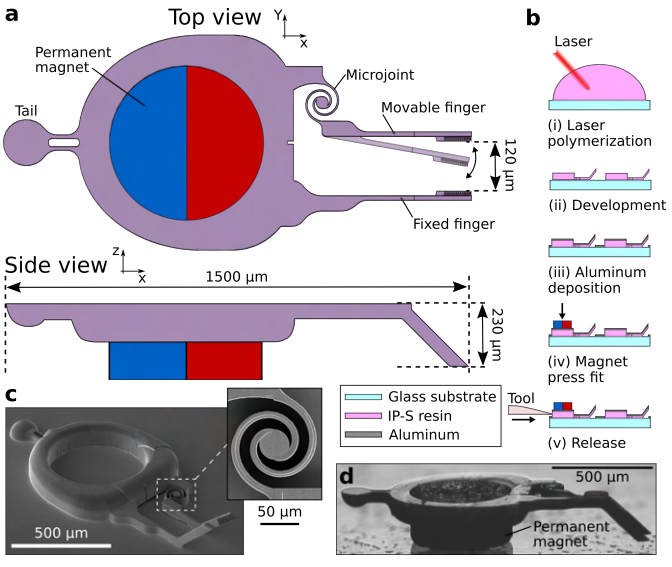

Fig. 2. Design and fabrication of the mobile microgripper. (a) Top view and side view of the proposed microgripper with its dimensions. (b) The full fabrication and release process of the microgripper. (c) SEM image of a fabricated microgripper before the release process. The inset shows a top view of the microjoint. (d) Image of a released microgripper with press fitted magnet.

cated by two-photon polymerization using IP-S resin on ITO-coated soda lime glass substrates. The bimaterial microjoint was realized by using two different printing laser powers to tune the physical properties of its materials. Then, the microgripper was developed in two PGMEA developer baths for 10 minutes and 20 minutes, respectively, to insure the removal of all residual resin. Finally, an aluminum layer of 600 nm was deposited by sputtering to increase the laser absorption. After fabrication, a diametrically-magnetized disk-shaped permanent magnet (Audemars Inc.) having a diameter of 500 µm and a thickness of 242 µm was press fitted manually in the body of the microgripper. Subsequently, the microgripper was released from the substrate by mechanical force. Fig. 2(c) shows a scanning electron microscope (SEM) image of a fabricated microgripper before the release process, where the inset shows a zoom-in image of the spiral bimaterial microjoint. Fig. 2(d) shows an image of a released microgripper with a press fitted magnet.

B. Magnetic Actuation

The goal of the magnetic actuation system is to remotely actuate the mobile microgripper with three degrees-of-freedom (DOF), i.e. 2D planar translation and in-plane rotation. Therefore, a system consisting of two pairs of electromagnets arranged orthogonally in the same plane is used to generate the desired magnetic field. The following mathematical modeling is based on [17]. A permanent magnet in an external non-uniform magnetic field experiences both a torque **T**, which controls the orientation of the magnet, and a force **F**, which controls the position of the magnet:

$$\mathbf{T} = V(\mathbf{M} \times \mathbf{B}) = (\mathbf{m} \times \mathbf{B}) \tag{1}$$

$$\mathbf{F} = V(\mathbf{M} \cdot \nabla)\mathbf{B} = (\mathbf{m} \cdot \nabla)\mathbf{B} \tag{2}$$

where V is the volume of the permanent magnet, **M** is its magnetization vector, **m** is the magnetic moment, and $\mathbf{B} \in \mathbb{R}^2$ is the magnetic field. Because a permanent magnet aligns its magnetization axis with the direction of the applied external magnetic field, its orientation can be controlled by specifying the field direction. In addition, by assuming that the electrostatic effects are negligible ($\nabla \cdot \mathbf{B} = 0$), and that no current is flowing at the working area ($\nabla \times \mathbf{B} = 0$), which is the case in this work, the augmented field and force equations can be expressed as:

$$\begin{bmatrix} \mathbf{B}(p) \\ \mathbf{F}(p,m) \end{bmatrix} = \begin{bmatrix} \mathbb{I}_2 & 0 \\ 0 & \mathbb{A}(m) \end{bmatrix} \begin{bmatrix} \mathbf{B}(p) \\ \mathbf{G}(p) \end{bmatrix} \tag{3}$$

where

$$\mathbf{B}(p) = \begin{bmatrix} B_x \\ B_y \end{bmatrix},\ \mathbf{F}(p,m) = \begin{bmatrix} F_x \\ F_y \end{bmatrix}$$

$$\mathbb{A}(m) = \begin{bmatrix} m_x & m_y & 0 \\ 0 & m_x & m_y \end{bmatrix},\ \mathbf{G}(p) = \begin{bmatrix} \frac{\partial B_x}{\partial x} \\ \frac{\partial B_x}{\partial y} \\ \frac{\partial B_y}{\partial y} \end{bmatrix}$$

where subscripts x, y represent vector components on the x-axis and y-axis respectively, matrix $\mathbb{A}(m)$ is the magnetization matrix that facilitates the dot product with **G**(p), which is the magnetic gradient matrix, p is the 2D position of the permanent magnet, B_x, B_y are the magnetic field components, F_x, F_y are the magnetic force components, m_x, m_y are the magnetic moment components, and $\mathbb{I}_2$ is the 2×2 identity matrix. Because of the linear relation between the magnetic field and the applied current through the electromagnets, it is convenient to describe the field as $\mathbf{B} = \hat{\mathbf{B}}\mathbf{I}$, where $\hat{\mathbf{B}}$ is the current-normalized magnetic field, and **I** is the current vector. As a result, the total magnetic field and magnetic gradient generated by the four electromagnets can be obtained by superimposing the field and gradient from individual electromagnets as follows:

$$\begin{bmatrix} \mathbf{B}(p) \\ \mathbf{G}(p) \end{bmatrix} = \begin{bmatrix} B_x \\ B_y \\ \frac{\partial B_x}{\partial x} \\ \frac{\partial B_x}{\partial y} \\ \frac{\partial B_y}{\partial y} \end{bmatrix} = \begin{bmatrix} \hat{B}_{1x} & \cdots & \hat{B}_{4x} \\ \hat{B}_{1y} & \cdots & \hat{B}_{4y} \\ \frac{\partial \hat{B}_1 x}{\partial x} & \cdots & \frac{\partial \hat{B}_4 x}{\partial x} \\ \frac{\partial \hat{B}_1 x}{\partial y} & \cdots & \frac{\partial \hat{B}_4 x}{\partial y} \\ \frac{\partial \hat{B}_1 y}{\partial y} & \cdots & \frac{\partial \hat{B}_4 y}{\partial y} \end{bmatrix} \begin{bmatrix} i_1 \\ \vdots \\ i_4 \end{bmatrix} = \mathbb{B}(p)\mathbf{I} \tag{4}$$

Consequently, Eq. (3) can be rewritten as:

$$\begin{bmatrix} \mathbf{B}(p) \\ \mathbf{F}(p,m) \end{bmatrix} = \begin{bmatrix} \mathbb{I}_2 & 0 \\ 0 & \mathbb{A}(m) \end{bmatrix} \mathbb{B}(p)\mathbf{I} \tag{5}$$

The expression in Eq. (4) requires the information about the magnetic field vector and its gradient at every position in the workspace. A number of method exist to acquire the field and gradient values including the magnetic dipole formula [17], finite element analysis (FEA) [18], and measurement-based interpolation [19]. In this work, the measurement-based interpolation method was adopted due to its fast calculation time and ease of implementation. For this, the working area of 10×10 mm was equally discretized into 10×10 discrete points and the 2D magnetic field components (B_x, B_y) were measured at each point for each individual electromagnet using a 3-axis Tesla meter (THM1176, Metrolab Technology SA, Switzerland) mounted on a motorized xy stage with micrometric accuracy. Subsequently, continuous 2D maps for magnetic fields and gradients for each electromagnet were acquired by interpolation.

Eq. (5) governs the relation between the input currents and the magnetic field and force vectors. Therefore, by taking the inverse of Eq. (5), the required current for each electromagnet for a given combination of orientation and position (i.e. magnetic field and force vectors) can be obtained. It is worth mentioning that Eq. (5)

produces a number of singularities for specific combinations of orientations and positions that causes its determinant to be zero [18]. These singular positions cause the currents supplying the electromagnets to reach very high values, which momentary disturbs the magnetic actuation and can cause an actuation failure. These singularities can be eliminated by increasing the number of electromagnets in the system to five, which is outside the scope of this paper. Therefore, the combinations of positions and orientations that result in a singularity were avoided as much as possible.

C. Laser Steering

The laser beam used to actuate the gripping mechanism of the mobile microgripper should be able to follow the position of the microjoint. Therefore, a laser steering system was developed to allow the optothermal actuation of the gripping mechanism on demand, as shown in Fig. 3(b). A tip/tilt galvo mirror was used to steer the laser beam on a 2D plane by specifying the desired x and y coordinates of the microjoint. The microjoint coordinates are obtained using image processing. However, when the laser strikes the microjoint, its position becomes difficult to obtain using image processing due to the high brightness of the laser. Therefore, the coordinates of the tail of the microgripper are first obtained and then transformed into the coordinates of the microjoint. The obtained microjoint coordinates are used as a reference to derive the position of the laser spot as follows:

$$\begin{bmatrix} l_x \\ l_y \end{bmatrix} = \mathbb{R}_z^2(\theta) \begin{bmatrix} l_{refx} \\ l_{refy} \end{bmatrix} \tag{6}$$

where l_x, l_y are the 2D laser spot coordinates, l_{refx}, l_{refy} are the 2D reference coordinates, and $\mathbb{R}_z^2(\theta)$ is the 2D rotation matrix. Consequently, the tip and tilt angles of the galvo mirror can be obtained as:

$$\begin{bmatrix} \theta_{tip} \\ \theta_{tilt} \end{bmatrix} = \begin{bmatrix} arctan(\frac{l_x}{d}) \\ arctan(\frac{l_y}{d}) \end{bmatrix} \tag{7}$$

where d is the distance from the galvo mirror to the microgripper. The tip and tilt angles are linearly related to the galvo mirror input voltages v_{tip}, v_{tilt}:

$$\begin{bmatrix} v_{tip} \\ v_{tilt} \end{bmatrix} = K_g \begin{bmatrix} \theta_{tip} \\ \theta_{tilt} \end{bmatrix} \tag{8}$$

where K_g is a scalar gain. This gain was tuned experimentally to have a minimum error between the reference position and the actual laser spot position. An f-theta lens was placed after the galvo mirror to focus the laser beam on a focal plane. Unlike conventional spherical focusing lenses that create a circular focal plane, f-theta lenses create a flat scanning field making it suited for laser scanning applications.

D. System Integration and Control

An experimental system is built as shown in Fig. 3(a). The system mainly consists of three modules: a magnetic actuation module, a laser steering module, and an observation module. The magnetic actuation module consists of two pairs of electromagnets (1300 turns, 17 mm long, 4 mm diameter ferromagnetic core) arranged orthogonally. The currents in the electromagnets are supplied by operational amplifiers (ST TL048CN, Texas Instruments Inc., US) connected to a power supply (AX 503, Metrix Inc.,France). These currents are controlled by the PC through a digital-analog converter (PCIe-6738, NI Inc., US). A three axis (x, y, θ) joystick with a push button is connected to the PC to allow the operator to control the mobile microgripper in subsequent micromanipulation experiments. The laser steering module consists of a continuous wave (CW) laser source (LAS-01087, Oxxius S.A., France) with a power of 60 mW and a wavelength of 532.1 nm. A galvo mirror (S335, Physik Instrumente GmbH & Co. KG, Germany) is placed on the laser path for laser steering. The laser beam is subsequently focused using an f-theta lens (S4LFT0063/121, Sill Optics GmbH & Co. KG, Germany) then reflected on a fixed right-angle mirror to strike the mobile microgripper, where the focused laser spot size was approximately 120 µm. The observation module consists of a microscope equipped with a high-speed camera (EoSens 4CXP, Mikrotron GmbH, Germany) with a frame rate of 500 fps and a resolution of 400×400 pixels. A notch filter (NF-25C05-40-532, Sigmakoki Inc., Japan) with a cutoff wavelength of 532 nm was mounted before the objective of the microscope to protect the camera from the laser beam. In addition, a laser line filter (VPFHT-25C-5320, Sigmakoki Inc., Japan) is placed under the working area to enhance the image contrast of the camera. The mobile microgripper is placed inside a solution of glycerin with 0.2% of surfactant (dish soap) on a glass substrate. The

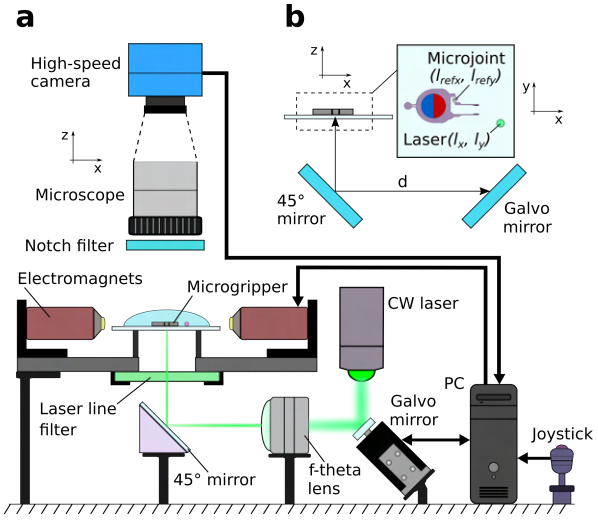

Fig. 3. (a) Diagram of the experimental system and its components. (b) Diagram explaining the 2D laser steering.

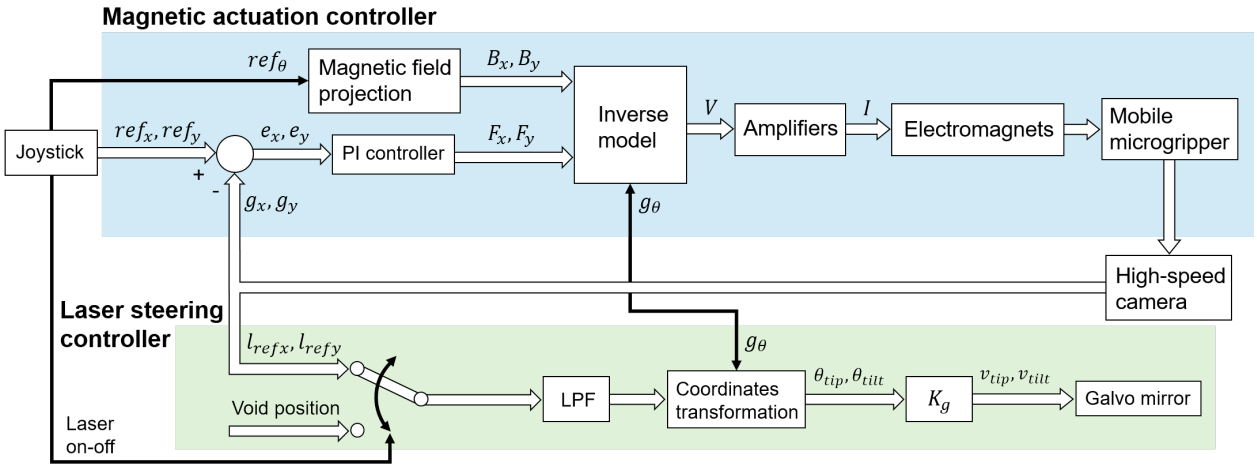

Fig. 4. Controller block diagram showing the magnetic actuation controller and the laser steering controller.

high viscosity of this solution enhances the mobility of the microgripper as it reduces the adhesion between the microgripper and the substrate.

The control block diagram of the full system is shown in Fig. 4. The controller is divided into two sub controllers: the magnetic actuation controller and the laser steering controller. The magnetic actuation controller uses a closed-loop to control the magnetic force (i.e. microgripper's position) and an open-loop to control the magnetic field (i.e. microgripper's orientation), which assumes that the microgripper aligns with the magnetic field direction [17]. The magnetic force control is based on a PI controller that uses the position of the microgripper (g_x, g_y) from the camera feedback to calculate the required force components that will be fed to the inverse of Eq. (5). In addition, the orientation feedback (g_θ) is used to calculate the x and y components of the magnetic moment of the microgripper, which will also be used in the inverse of Eq. (5). The high-speed image feedback (500 Hz) enhances the control performance compared to conventional image feedback (30 Hz) by allowing a 2 ms control frequency. The image processing is achieved using a simple and fast algorithm that makes use of the small differences between consecutive image frames [20]. The laser steering controller uses an open-loop to control the tip/tilt angles of the galvo mirror. Here, the position of the microjoint in the microgripper is calculated at each image frame and used as a reference position for the controller. A low pass filter (LPF) is used to reduce the vibrations of the laser spot caused by the image processing noise. In micromanipulation experiments, the joystick is used to generate the reference position and orientation of the microgripper and to control the on-off activation of the laser beam by switching between the microjoint coordinates and a void position using a push button.

III. EXPERIMENTS

A. Optothermal Actuation of Microgripper

In this section, the laser actuation of the microgripper by utilizing its optothermal response is confirmed. Here, laser heating is applied for two seconds on a stationary microgripper that is placed inside the glycerin solution to initiate its open and close motion, as shown in Fig. 5(a) (see the attached video). The microgripper is initially in an open state without any laser heating. Upon laser heating of the spiral microjoint, the movable arm of

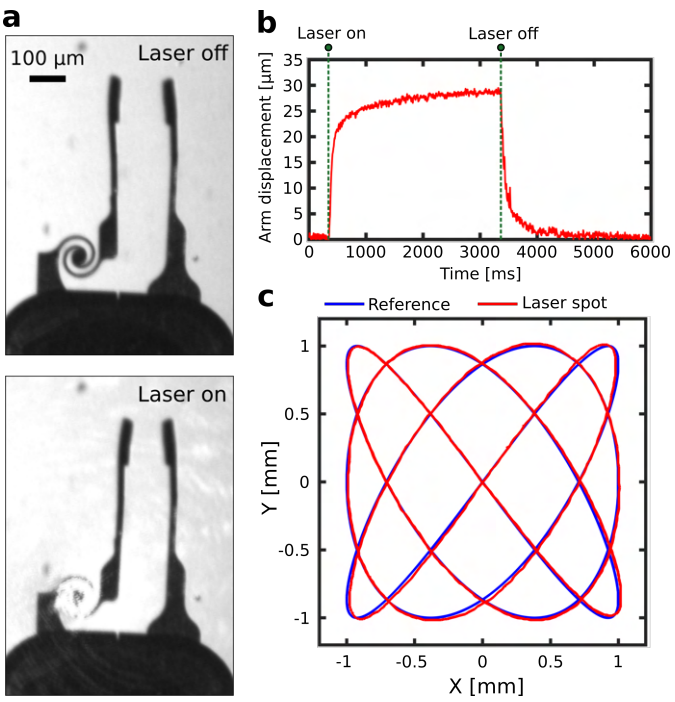

Fig. 5. Optothermal actuation of the microgripper showing its open and close states. (b) Step response of the gripping mechanism. (c) Performance of the laser steering system through a path following experiment of a Lissajous curve. The blue and red lines show the reference trajectory and the position of the laser spot, respectively.

the microgripper is actuated and the closed state of the microgripper is realized. The initial gap between the two fingers of the microgripper is approximately 120 µm (open) and then decreased to approximately 85 µm (close) by laser heating, resulting in a maximum displacement of 35 µm. In addition, the time response of the gripping mechanism is confirmed by obtaining its step response, as shown in Fig. 5(b). Here, the laser is applied for three seconds and the induced displacement of the movable arm is sampled at a frequency of 250 Hz. The time constant of the step response, i.e. the time to reach 63% of the steady-state value, is approximately 100 ms. The slower time response compared to our previous work [16] is mainly due to the higher viscosity of glycerin compared to air and water. Nonetheless, the achieved response is relatively fast and appropriate for the required micromanipulation application. In terms of force, the microjoint that is used to actuate the gripping mechanism can generate forces in the order µN [16]. Therefore, a similar force range can be expected in the proposed microgripper.

Next, path following experiments for laser steering are conducted to confirm its ability to dynamically follow the position of the microgripper. A Lissajous curve is used as a reference trajectory for the laser spot and image processing is used to detect and register its position (see the attached video). Optical neutral density filters are used to reduce the laser power, and thus its brightness, to enhance the detection of the laser spot position. Fig. 5(c) shows the experimental results where the blue line shows the reference trajectory and the red line shows the actual position of the laser spot. The experiments show that the positioning error of the laser steering is approximately 25 µm when the mean speed of the laser spot is 0.4 mm/s. Taking into account the diameter of the microjoint (130 µm) and the average speed of mobile microgrippers [5], the experimental results are suitable for actuating the gripping mechanism and to continuously track the microgripper in any position within the working area.

B. Magnetic Actuation Performance

Path following experiments are conducted to verify the performance of the magnetic actuation system. In these experiments, a dummy mobile microgripper that consists of only the body part is used for simplicity. To first verify the performance of the position control, the mobile microgripper is controlled by magnetic actuation to follow a circular reference trajectory with a diameter of 1 mm for three continuous cycles, while applying a constant orientation of 45° (see the attached video). This reference trajectory does not pass through any singular positions. The maximum magnetic field strength is set to 2 mT and is used for all subsequent magnetic actuation experiments. Fig. 6(a) shows the experimental results where the blue line shows the reference trajectory and the red line shows the actual position of the microgripper. From the experiment, the positioning error, i.e. the difference between the position of the microgripper and the reference trajectory, has a mean value of 6 µm, a maximum value of 13 µm, and a standard deviation of 2.5 µm. The error values are less than 1% of the total size of the microgripper, which shows the high accuracy of the magnetic actuation and confirms its suitability for the required micromanipulation tasks. Furthermore,

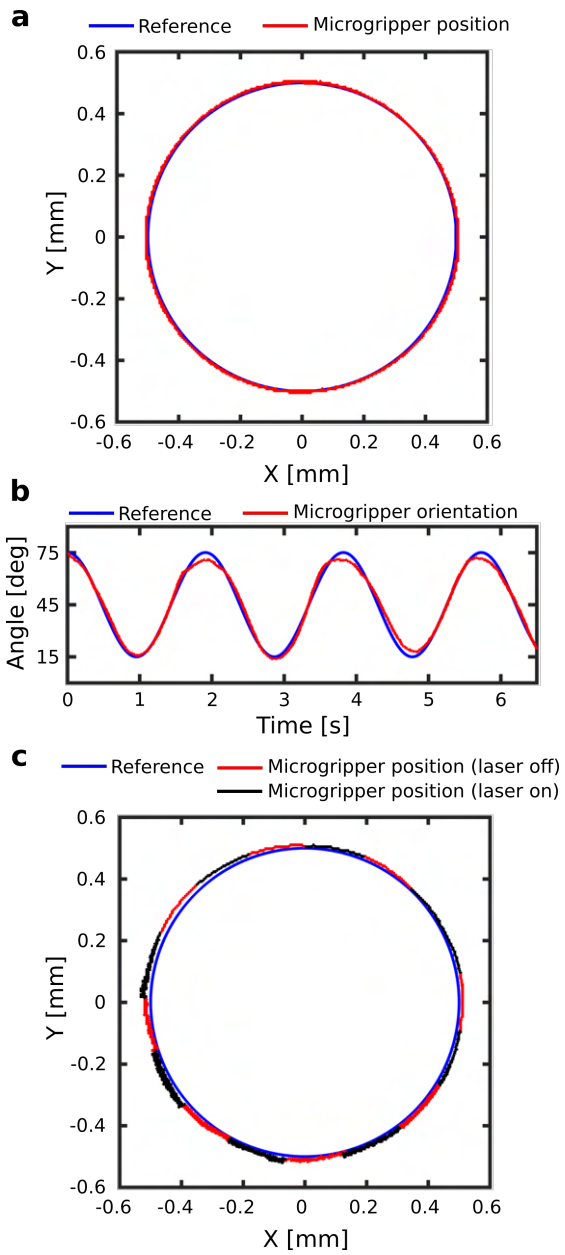

Fig. 6. Performance of the magnetic actuation system. (a) Path following of a circular trajectory. (b) Orientation control using a sinusoidal trajectory. The blue and red lines show the reference trajectory of the magnetic actuation and the position or orientation of the microgripper, respectively. (c) The effect of laser optothermal actuation on magnetic actuation showing the path following of the magnetically actuated microgripper while laser heating is applied periodically with a frequency of 0.5 Hz. The blue, red, and black lines show the reference trajectory of the magnetic actuation, the position of the microgripper in case of laser heating, the position of the microgripper in case of no laser heating, respectively.

the mean speed of the microgripper is 0.1 mm/s. This speed is chosen to prevent high overshoot values of the magnetic controller in case of a temporary adhesion between the microgripper and the glass substrate, which enhances the positioning accuracy. Next, the orientation control is evaluated by applying a sinusoidal reference magnetic field direction covering a range of 60°. This reference orientation does not pass through any singular positions. Fig. 6(b) shows the experimental results where the blue line shows the reference orientation and the red line shows the actual orientation of the microgripper. The controller is capable of orienting the microgripper in the direction of the magnetic field with a relatively low orientation error of approximately 2°, which is sufficient for the proposed applications.

The full decoupling between the positioning and the gripping mechanism actuation of the mobile microgripper is one of the main advantages of hybrid actuation. Therefore, the magnetic actuation should not be affected by simultaneously applying optothermal actuation. The decoupling is confirmed experimentally by applying a periodic optothermal activation of the gripping mechanism with a frequency of 0.5 Hz while magnetically positioning the microgripper along a circular trajectory with a diameter of 1 mm (see the attached video). Fig 6(c) shows the results of positioning the microgripper along the X-axis and Y-axis using magnetic actuation, where the reference trajectory is shown in blue and the actual position is shown in red and black. The red line shows the actual position of the microgripper while the laser is steered to a void position (-1,-1) outside the working area i.e. no optothermal activation of the gripping mechanism. The black line shows the actual position of the microgripper while the laser is following the microjoint position, i.e. optothermal activation of the gripping mechanism. The mean positioning error of the magnetic actuation in this experiment is 12 µm, which is is still below 1% of the total size of the microgripper. This confirms that the optothermal activation of the gripping mechanism does not affect the accuracy of the magnetic actuation, thus a fully decoupled actuation is realized.

C. Application to Micromanipulation

Finally, to confirm the performance of the mobile microgripper in micromanipulation applications, a pick-and-place experiment of a 95 µm microbead is performed in liquid. The microbeads are placed in the glycerin solution with the microgripper on a glass substrate. The three axis joystick is used by the operator to control the planar position and orientation of the microgripper through magnetic actuation. In addition, the push button of the joystick is used to switch the reference command of the laser steering controller between the position of the microgripper and the void position outside the working area, which allows the user to initiate the optothermal actuation of the microgripper on demand. To record the experiment, a 5 MP CMOS camera (GO-5000C-USB, JAI Ltd., Denmark) is attached to the microscope using an image splitter. This camera is connected to a separate laptop PC to maintain the control frequency of the control PC, where directly saving the frames of the high-speed camera would increase the computational time. Fig. 7 demonstrates the results of the pick-and-place experiment with the time stamp of each step. First, the mobile microgripper is actuated to the position of the target microbead while having the gripping mechanism in an open state, as shown in Fig. 7(a-b). Next, the gripping mechanism is switched to a closed state by the laser to catch the microbead, as shown in Fig. 7(c). The microbead is then manipulated to a new position in the working area while being gripped by the microgripper, as shown in Fig. 7(d). Subsequently, the gripping mechanism is switched back to an open state to release the microbead, as shown in Fig. 7(e). Finally, the microgripper is actuated away from the microbead to confirm its successful release, as shown in Fig. 7(f).

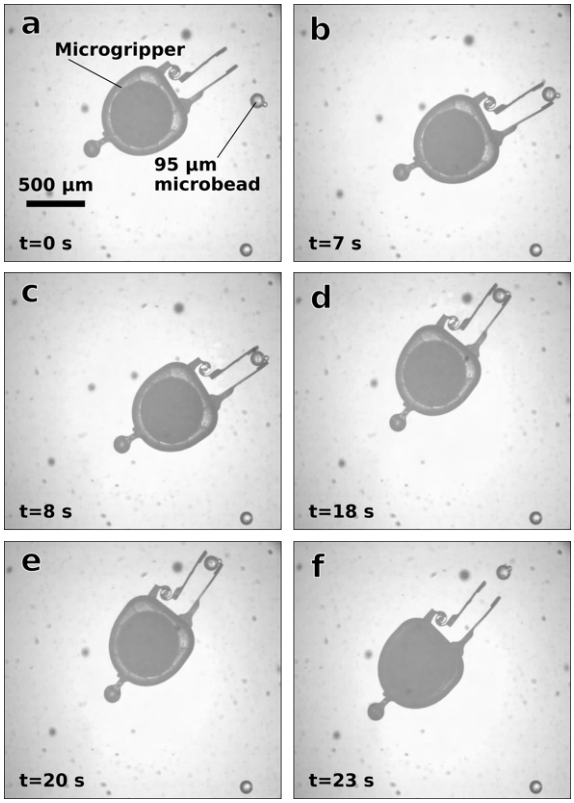

Fig. 7. In-liquid pick-and-place of a 95-µm diameter microbead using the proposed mobile microgripper. See the attached video.

It was observed in the experiment that the high viscosity of glycerin can have a negative effect on the gripping process due to higher viscous drag on both the gripper fingers and the manipulated object. This can occasionally cause the manipulated microbead to be released even when the gripping mechanism is in a closed state. Therefore, the use of less viscous liquids such as water-based solutions can be considered in future

work. This would also enable biomedical applications such as cell manipulation, where most cell culture media are water-based. However, when using water-based solutions, the adhesion forces between the microgripper and the substrate of the working area increases, which reduces the performance of the magnetic actuation. Therefore, a number of solutions can be investigated including surface coating and structural designs with a small contact area [21] to reduce the adhesion in water-based environments in future work. Alternatively, gripping mechanisms that generate higher forces such as bistable mechanisms can be also investigated.

IV. CONCLUSIONS

We proposed a compelling proof of concept of a mobile microgripper that is actuated using a hybrid scheme for in-liquid micromanipulation. Magnetic actuation was used to position the microgripper in the working area, while laser optothermal actuation was used to control the gripping mechanism. The developed microgripper could realize a gripping motion with a maximum displacement of 35 µm and a response time of 100 ms. In addition, magnetic actuation of the microgripper was realized with an accuracy of 6 µm for translation and 2° for rotation. The laser was steered to track the microgripper with an accuracy of 25 µm. The full decoupling between optothermal and magnetic actuation was also verified. Finally, the performance of the mobile microgripper was shown through a successful pick-and-place experiment of a 95-µm diameter microbead inside a glycerin solution.

The use of bulky permanent magnets increases the footprint of the microgripper. Therefore, the use of magnetic nanoparticles inside the resin in the fabrication process or selectively depositing of a magnetic film on the microgripper's body would result in a miniaturized and monolithic microgripper in future work. This would also reduce the fabrication complicity by removing the need for microassembly. Further miniaturization (e.g. below 100 µm) is limited due to fabrication constraints and would require the development of a more compact microjoint for the gripping mechanism. The proposed mobile microgripper has a high potential to be evolved into complex mobile microtools by utilizing multiple microjoints. For instance, instead of a gripping mechanism with only one DOF, microtools with multiple DOF can be implemented and controlled by temporally multiplexing the laser beam between multiple microjoints. This can have a high impact on challenging biomedical applications including cell positioning and rotation, cell surgery, and embryo biopsy.

References

[1] M. Leveziel, W. Haouas, G. J. Laurent, M. Gauthier, and R. Dahmouche, "Migribot: A miniature parallel robot with integrated gripping for high-throughput micromanipulation," *Science Robotics*, vol. 7, no. 69, p. eabn4292, 2022.

[2] Z. Zhang, Y. Yu, P. Song, Y. Zhang, D. Tian, H. Zhang, H. Wei, M. Cui, G. Si, and X. Zhang, "Automated manipulation of zebrafish embryos using an electrothermal microgripper," *Microsystem Technologies*, vol. 26, no. 6, pp. 1823–1834, 2020.

[3] Z. Lyu and Q. Xu, "Recent design and development of piezoelectric-actuated compliant microgrippers: A review," *Sensors and Actuators A: Physical*, vol. 331, p. 113002, 2021.

[4] C. Yin, F. Wei, Z. Zhan, J. Zheng, L. Yao, W. Yang, and M. Li, "Untethered microgripper-the dexterous hand at microscale," *Biomedical microdevices*, vol. 21, no. 4, pp. 1–18, 2019.

[5] B. Ahmad, M. Gauthier, G. J. Laurent, and A. Bolopion, "Mobile microrobots for in vitro biomedical applications: A survey," *IEEE Transactions on Robotics*, 2021.

[6] C. Hu, S. Pané, and B. J. Nelson, "Soft micro-and nanorobotics," *Annual Review of Control, Robotics, and Autonomous Systems*, vol. 1, pp. 53–75, 2018.

[7] E. Diller and M. Sitti, "Three-dimensional programmable assembly by untethered magnetic robotic micro-grippers," *Advanced Functional Materials*, vol. 24, no. 28, pp. 4397–4404, 2014.

[8] J. Zhang, O. Onaizah, K. Middleton, L. You, and E. Diller, "Reliable grasping of three-dimensional untethered mobile magnetic microgripper for autonomous pick-and-place," *IEEE Robotics and Automation Letters*, vol. 2, no. 2, pp. 835–840, 2017.

[9] J. S. Randhawa, T. G. Leong, N. Bassik, B. R. Benson, M. T. Jochmans, and D. H. Gracias, "Pick-and-place using chemically actuated microgrippers," *Journal of the American Chemical Society*, vol. 130, no. 51, pp. 17238–17239, 2008.

[10] H. Jia, E. Mailand, J. Zhou, Z. Huang, G. Dietler, J. M. Kolinski, X. Wang, and M. S. Sakar, "Universal soft robotic microgripper," *Small*, vol. 15, no. 4, p. 1803870, 2019.

[11] K. Kobayashi, C. Yoon, S. H. Oh, J. V. Pagaduan, and D. H. Gracias, "Biodegradable thermomagnetically responsive soft untethered grippers," *ACS applied materials & interfaces*, vol. 11, no. 1, pp. 151–159, 2018.

[12] J. C. Breger, C. Yoon, R. Xiao, H. R. Kwag, M. O. Wang, J. P. Fisher, T. D. Nguyen, and D. H. Gracias, "Self-folding thermomagnetically responsive soft microgrippers," *ACS applied materials & interfaces*, vol. 7, no. 5, pp. 3398–3405, 2015.

[13] C. Pacchierotti, F. Ongaro, F. van den Brink, C. Yoon, D. Prattichizzo, D. H. Gracias, and S. Misra, "Steering and control of miniaturized untethered soft magnetic grippers with haptic assistance," *IEEE Transactions on Automation Science and Engineering*, vol. 15, no. 1, pp. 290–306, 2018.

[14] C. R. Dunn, B. P. Lee, and R. M. Rajachar, "Thermomagnetic-responsive self-folding microgrippers for improving minimally invasive surgical techniques and biopsies," *Molecules*, vol. 27, no. 16, p. 5196, 2022.

[15] C. Elbuken, M. B. Khamesee, and M. Yavuz, "Design and implementation of a micromanipulation system using a magnetically levitated mems robot," *IEEE/ASME Transactions on Mechatronics*, vol. 14, no. 4, pp. 434–445, 2009.

[16] B. Ahmad, A. Barbot, G. Ulliac, and A. Bolopion, "Remotely actuated optothermal robotic microjoints based on spiral bimaterial design," *IEEE/ASME Transactions on Mechatronics*, vol. 27, no. 5, pp. 4090–4100, 2022.

[17] J. J. Abbott, E. Diller, and A. J. Petruska, "Magnetic methods in robotics," *Annual Review of Control, Robotics, and Autonomous Systems*, vol. 3, no. 1, pp. 57–90, 2020.

[18] O. Erin, S. Raval, T. J. Schwehr, W. Pryor, Y. Barnoy, A. Bell, X. Liu, L. O. Mair, I. N. Weinberg, A. Krieger, and Y. Diaz-Mercado, "Enhanced accuracy in magnetic actuation: Closed-loop control of a magnetic agent with low-error numerical magnetic model estimation," *IEEE Robotics and Automation Letters*, vol. 7, no. 4, pp. 9429–9436, 2022.

[19] A. J. Petruska, J. Edelmann, and B. J. Nelson, "Model-based calibration for magnetic manipulation," *IEEE Transactions on Magnetics*, vol. 53, no. 7, pp. 1–6, 2017.

[20] B. Ahmad, H. Maeda, T. Kawahara, and F. Arai, "Microrobotic platform for single motile microorganism investigation," *Micromachines*, vol. 8, no. 10, p. 295, 2017.

[21] M. Hagiwara, T. Kawahara, T. Iijima, and F. Arai, "High-speed magnetic microrobot actuation in a microfluidic chip by a fine v-groove surface," *IEEE Transactions on Robotics*, vol. 29, no. 2, pp. 363–372, 2012.